Biosensors and Bioelectronics 163 (2020) 112281

Contents lists available at ScienceDirect

Biosensors and Bioelectronics

journal homepage: http://www.elsevier.com/locate/bios

Nanochannel-driven rapid capture of sub-nanogram level biomarkers for painless preeclampsia diagnosis

Ye-Eun Kang [a], Keum-Yong Seong [a], Sang-Gu Yim [a], Yechan Lee [a], Sung-Min An [a], Seung Chul Kim [b], Kyujung Kim [c], Beum-Soo An [a], Kyu-Sup Lee [b], Seung Yun Yang [a,*]

[a] Department of Biomaterials Science, Pusan National University, Miryang, 50463, Republic of Korea
[b] Department of Obstetrics and Gynecology, Pusan National University School of Medicine, Busan, 49241, Republic of Korea
[c] Department of Cogno-Mechatronics Engineering, Pusan National University, Busan, 46241, Republic of Korea

ARTICLE INFO

Keywords:
Biosensor
Preeclampsia
Microneedle
Immunoassay
Painless diagnosis

ABSTRACT

Preeclampsia (PE) is a pregnancy-specific hypertensive syndrome recognized as the leading cause of maternal and fetal morbidity and mortality worldwide. Painful blood-collection procedures or low accuracy of non-invasive approaches require faster, patient-friendly, and more sensitive diagnostic technologies. Here we report a painless, highly sensitive detection platform using nanoporous microneedles (nMNs) that enables rapid capture of biomarkers present at sub-nanogram levels. The highly porous nanostructures on the nMN surface were prepared by anodization of aluminum MN and then functionalized by immobilization of capture antibodies to detect target biomarkers based on an immunoassay method. The immuno-functionalized nMN array demonstrated rapid capture of an estrogen (E2) biomarker for PE following a 1-min incubation and exhibited a concentration-dependent change in fluorescence intensity over the E2 range of 0.5 ng mL^{-1} to 1000 ng mL^{-1} after treatment with fluorescence-detection antibodies. Remarkably, the nMN patch selectively detected sub-nanogram-levels of E2 in subcutaneous interstitial fluid from rats with increased diagnostic accuracy as compared with commercial immunoassay kits. This bio-functionalized nMN platform showed improved biosensing capability for multiple PE-related biomarkers, including hormones and proteins. Furthermore, this painless method demonstrated efficacy as a point-of-need diagnostic platform using portable smartphone-based fluorescence microscope to obtain fluorescence images of biomarker-captured nMN arrays.

1. Introduction

Preeclampsia (PE) is a pregnancy-specific, hypertensive disorder affecting 3%–8% of pregnancies worldwide and a leading cause of maternal and perinatal morbidity and mortality (Anderson et al., 2012; Venkatesha et al., 2006). Although the cause of PE remains unclear, obstruction of blood supply to the placenta during the developmental stage after placental implantation could result in increased blood pressure and damage to multiple organs (Tian et al., 2016). Although the onset of PE is often asymptomatic, it can be characterized by hypertension and proteinuria after 20 weeks of gestation (O'Gorman et al., 2016b). Clinical symptoms related to PE appear late, but recent studies show that early diagnosis of PE is possible by assessing maternal factors and biomarkers (O'Gorman et al., 2016; Poon and Nicolaides, 2014), such as PE-related RNA (O'Gorman et al., 2016b), enzymes (Baumann et al., 2008; O'Gorman et al., 2016b), and hormones (Shin et al., 2018). A recent study found that plasma concentrations of the female sex hormone [estradiol (E2), a predominant estrogen subtype generated during the reproductive years] in women with PE are 5-fold lower than those in normal pregnant women (PE: 2.9 ± 1.9 ng mL^{-1} vs. normal: 10.5 ± 1.8 ng mL^{-1}), suggesting E2 as a potential biomarker for PE diagnosis (Shin et al., 2018). Because medication for PE prevention is only effective at ≤ 16 weeks of gestation, early diagnosis is important (Bujold et al., 2010).

To analyze biomarkers for PE diagnosis, blood is usually sampled using a hypodermic syringe; however, this method is invasive, painful, inconvenient to patients, and requires trained professionals. Additionally, because the collected blood sample requires multiple rounds of processing in a clinical laboratory, this becomes a time-consuming and costly diagnostic process. Non-invasive methods for PE diagnosis are mainly associated with measurement of blood pressure in maternal blood vessels that supply the uterus (O'Gorman et al., 2016b). Because

* Corresponding author.
E-mail address: syang@pusan.ac.kr (S.Y. Yang).

https://doi.org/10.1016/j.bios.2020.112281
Received 24 January 2020; Received in revised form 28 April 2020; Accepted 6 May 2020
Available online 11 May 2020

increased blood pressure due to poor placental perfusion is related to PE development (Redman and Sargent, 2005; Roberts and Cooper, 2001; Roberts and Hubel, 2009), this simple approach is effective at detecting placental impairment for PE diagnosis. However, accurate assessment of PE can be challenging, because each individual exhibits considerable variability.

Recently, patch-type microneedle (MN) arrays were developed to effectively extract and/or detect biomarkers in tissue interstitial fluids (ISFs) with minimal pain. Swellable MNs capable of absorbing body fluids potentially containing biomarkers or surface-functionalized solid MNs coated with biomarker-capturing probes have been successfully used (Coffey et al., 2013, 2018; Corrie et al., 2010; Muller et al., 2012). The swellable MN array prepared using cross-linked hydrophilic polymers was demonstrated as efficacious for detecting biomarkers, although it is difficult to apply as a rapid detection platform due to the MN-swelling kinetics that accompany fluid uptake (Chang et al., 2017; Mandal et al., 2018; Romanyuk et al., 2014). As another approach, surface-functionalized solid MNs have been applied in diverse biosensing systems using electrochemical or optical transduction methods, depending on the target molecules (Bollella et al., 2019; Coffey et al., 2013, 2018; Gholami et al., 2019; Gowers et al., 2019; Hwa et al., 2015; Jin et al., 2019; Keum et al., 2015; Li et al., 2015a; Liu et al., 2019; Mohan et al., 2017; Muller et al., 2012). For example, metal MN arrays with an electro-conductive surface-layer trapping active enzyme (glucose oxidase) demonstrated real-time sensing capability of glucose in the millimolar range (Chinnadayyala et al., 2018). Additionally, antibody-coated solid MNs selectively captured target biomarkers from skin ISFs with good sensitivity, enabling diagnosis of various diseases, including influenza and dengue infection (Coffey et al., 2013, 2018; Corrie et al., 2010; Muller et al., 2012). However, their detection limits were insufficient for nanogram-level biomarkers, which is a clinical requirement for diagnosing diseases, including PE.

A suitable platform capable of overcoming the limitations of existing diagnostic platforms, including those for PE diagnosis, should be 1) sensitive enough to detect biomarkers at sub-nanogram levels, 2) capable of providing rapid biomarker collection or capture capability comparable to that of blood collection with a syringe, 3) simple to use in a low-cost and scalable format, 4) minimally invasive enough to promote patient compliance, and 5) capable of integration into a portable diagnostic system for point-of-care testing.

In this study, we designed a painless, highly sensitive detection platform using nanoporous MN (nMN) patches capable of rapidly capturing biomarkers occurring at sub-nanogram levels. The nMNs were functionalized with an antibody to selectively capture E2 (a PE biomarker) following insertion into the skin, thereby enabling PE diagnosis by measuring biomarker concentrations based on an immunoassay method (Fig. 1). To provide an ultrahigh density of binding sites enabling detection of trace amounts of target analyte in subcutaneous ISFs, we created a uniform nanoporous structure on tissue-penetrating aluminium (Al) MN arrays by controlled anodization. The rapid, sub-nanogram-level sensing capability of the immuno-functionalized nMN patches was verified by *in vitro* E2 detection tests and *in vivo* using experimental animals following application to the skin for 1 min.

2. Materials and methods

2.1. Fabrication of nMNs by anodization

The bullet-shaped Al MN array was manufactured by a milling process using a computer numerical-control machine. The Al MNs were first degreased in acetone for 5 min through sonication, followed by electrochemical polishing at 20 V in an ethanol/perchloric acid mixture (4:1, vol%) at 7 °C for 30 s. The MNs were then washed with ethanol, dried with N_2, and anodized in aqueous oxalic acid solution (0.3 M) at 15 °C and 40 V for 3 h. After anodization, the pore size was expanded by immersion in 0.1 M phosphoric acid solution at 30 °C for 25 min (Yang et al., 2012). The nMNs and non-porous MNs were characterized using an optical microscope (Eclipse TS100; Nikon, Tokyo, Japan) to determine their length, tip angle, tip diameter, and base diameter. The nanoporous structure of anodized MNs was evaluated using a field-emission scanning electron microscope (FE-SEM, Hitachi S-4700; Hitachi, Tokyo, Japan) at a 10-kV working voltage, following platinum coating using an ion sputter coater (Hitachi E-1010; Hitachi) for 40 s. The surface area of the nMNs was estimated using the unit cell structure of anodic aluminium oxide (AAO) (see Supplementary Material).

2.2. Measurement of the insertion force into porcine skin

A displacement-force test station (Universal Testing Machine A&D 5000H; A&D Sales Corp., Seoul, Korea) was used to measure the force applied to a needle and the needle position during the sequence of needle translation to the skin, deflection of tissue around the needle, and

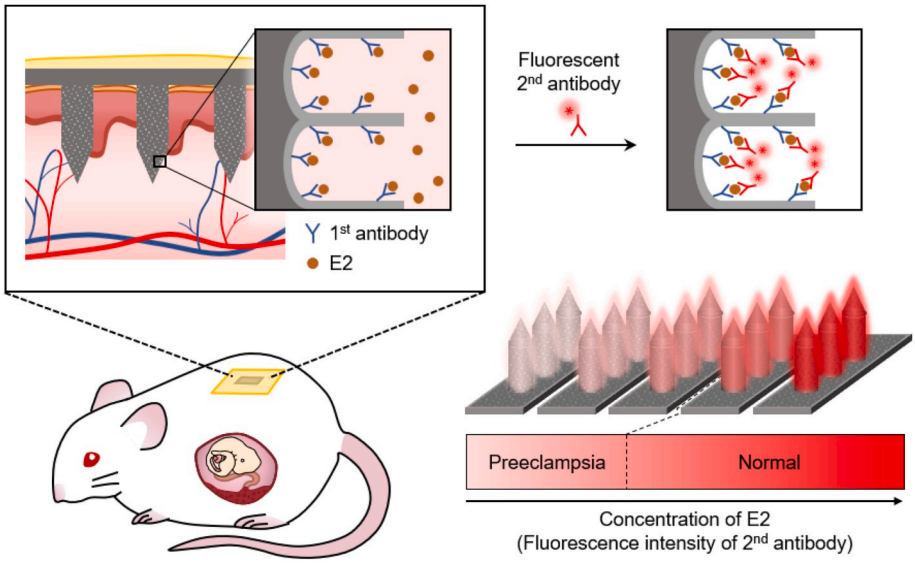

Fig. 1. Schematic illustration of the immuno-functionalized nMN patch used to diagnose PE through detection of an E2 biomarker. Sub-nanogram levels of E2 can be captured from subcutaneous ISFs by biomarker-specific probes immobilized on the surface of high-density nanopores and quantified by immunoassay to allow PE diagnosis.

insertion into porcine skin (Davis et al., 2004). The applied speed into the porcine skin was 10 mm/min. Porcine skin was dried at 37 °C for 15 min to obtain a similar level of humidity and elasticity relative to that in human skin.

2.3. Immuno-functionalization of nMNs

The probe antibody for E2 was electrostatically immobilized to nMNs after surface modification. The nMN patch was first cleaned in acetone for 10 min, followed by treatment with O_2 plasma to generate negative charges on the nMN surface. The negatively charged nMNs were then immersed in aqueous solution (0.6 w/v%) of positively charged poly (allylamine hydrochloride) (PAH, MW: 15 kDa) for 10 min. After coating, the nMN patch was immersed in deionized water for 10 min and dried with N_2, followed by casting of the positively charged 1st antibody [1st Ab, 17-β estradiol antibody (5E500); Santa Cruz Biotechnology, Dallas, TX, USA) in carbonate buffer (0.2 M sodium carbonate/bicarbonate buffer, pH 9.4] on each nMN (2 μL per needle) and incubation for 1 h. The nMN patch was washed six times in phosphate-buffered saline with 0.05 wt% Tween-20 (PBST) to remove excess antibody. To reduce nonspecific binding at the interface, each nMN was treated with 2 μL of 5% bovine serum albumin (BSA) in PBST blocking buffer and incubated for 1 h, followed by washing of the MN patch six times with PBST.

The surface charge of the O_2-plasma-treated and PAH-coated MNs and the 1st Ab was assessed by zeta-potential measurements under different pH conditions using a zeta-potential measurement system (ELS-Z 2000; Otsuka Electronics, Osaka, Japan) and the Malvern Zetasizer (Zetasizer Nano ZS; Malvern Instruments, Malvern, UK). To measure the surface charge of the nMN, a nanoporous Al sheet with the same chemical composition was used. The nMN surface at each of the coating steps was imaged by FE-SEM (Hitachi S-4700; Hitachi).

2.4. Optimization of nMNs for E2 capture

To determine the appropriate concentration of the 1st Ab, each PAH-coated nMN patch was treated with 2 μL of 1st Ab (10 μg mL^{-1}, 20 μg mL^{-1}, and 50 μg mL^{-1} in carbonate buffer) per a nMN, followed by incubation for 1 h. The nMN patches were then washed six times with PBST and treated with 2 μL of BSA per needle. The nMNs were then treated with 2 μL of E2 solution [10 ng mL^{-1} dissolved in 0.1% dimethyl sulfoxide (DMSO) in PBS] per needle and incubated for 30 min. The nMN patch was then washed six times with PBST to remove any excess, followed by treatment of each MN with 20 μg mL^{-1} of Texas Red (TR)-labeled secondary antibody (TR-2nd Ab; goat anti-mouse IgG (H + L) cross-adsorbed secondary antibody, Texas Red-X; Invitrogen, Carlsbad, CA, USA) in PBS (2 μL per needle) and incubation for 1 h. The nMN patch was then washed six times in PBST to remove unbound antibodies. To assess the E2-capturing ability of the nMNs according to incubation time, each BSA/1st Ab-treated (treated with 20 μg mL^{-1} of 1st Ab and BSA) nMN patch was then treated with 1 ng mL^{-1} and 10 ng mL^{-1} of E2 solution (2 μL per needle) and incubated for 1, 10, and 30 min. The nMN was then washed and treated with the TR-2nd Ab, as described, followed by washing six times with PBST.

2.5. In vitro E2-capture tests using immuno-functionalized nMNs

To investigate the detection limit of the nMN, each of the BSA/1st Ab-treated nMN and non-porous MN patches was treated with 2 μL of E2 solution (0 ng mL^{-1} to 1000 ng mL^{-1} of E2 dissolved in 0.1% DMSO in PBS) per needle and incubated for 1 and 30 min. All nMN surfaces were imaged by FE-SEM (Hitachi S-4700; Hitachi). To examine trapping and selective binding of the 2nd Ab, the BSA/1st Ab-treated nMN patch was treated with 2 μL of the TR-2nd Ab and TR-labeled dextran (TR-dex; Invitrogen) at 1 ng mL^{-1}, 10 ng mL^{-1}, and 1000 ng mL^{-1} of each solution per needle. The nMN patches were then incubated for 1 h and washed six times with PBST.

2.6. Animals and care

The protocol for the animal experiment was reviewed and approved by the Institutional Animal Care and Use Committee (PNU-2018-2094) of Pusan National University. Female Sprague−Dawley rats (10 weeks old) were purchased from Samtako-Bio Korea (Osan, Korea) and housed under standard laboratory conditions with controlled temperature/humidity, a 12-/12-h light/dark cycle, and free access to food and water at the Pusan National University Laboratory Animal Resources Center, which is accredited by the Korea Food and Drug Administration in accordance with the Laboratory Animal Act (Accredited Unit Number: 000231) and AAALAC International according to the National Institutes of Health guidelines (Accredited Unit Number: 001525).

2.7. In vivo E2-capture tests using immuno-functionalized nMNs

The ability of nMNs to capture E2 present in rats was determined in normal and E2-injected animal groups. To prepare nMN patches for *in vivo* application, a nMN array (1 x 5 MN) was partially embedded in the disc-type polydimethylsiloxane (PDMS) pad (1.5 cm wide, 0.2 cm deep) and then attached to a hydrocolloid adhesive (3 × 3 cm^2) for skin adhesion (Fig. S1). The animals were acclimatized to laboratory conditions for 7 days before the experiment. Experimental procedures were performed under Zoletil (Virvac, Carros, France)/Alfaxan (Jurox, Rutherford, Australia) anesthesia. Back hair was removed using an electric clipper and shaving wax under anesthesia. Animals were divided into the following two groups ($n = 3$/group): 1) normal rats; BSA/1st Ab-treated nMNs and non-porous MNs and BSA-treated nMNs (without 1st Ab) were applied to the dorsal skin; and 2) E2-injected rats; E2 solution was intravenously administered *via* a tail vein, and BSA/1st Ab-treated nMNs and non-porous MNs were applied to the dorsal skin. E2 solution was injected into rats in order to ensure an E2 concentration in the blood of 10 ng mL^{-1}. To enhance circulating biomarkers (E2) in the upper dermis or epidermis, the dorsal skin was illuminated by heating lamp (OSRAM Dulux superstar 20 W/860) for 10 min. The MN patches inserted in the rat skin were incubated for 1 min, followed by washing six times with PBST. Following removal, the MN patches were treated with the TR-2nd Ab, as described, followed by washing six times with PBST.

2.8. Hematological & serum biochemistry analysis

To analyze hematology and biochemistry, blood samples were collected after necropsy *via* the abdominal vein. For hematology, whole-blood samples were added to complete blood count (CBC) bottles [Ethylenediaminetetraacetic acid (EDTA) tubes; Green Cross Medical Industry, Yongin, Korea]. Hematological parameters were analyzed using a hematology automatic analyzer (US/Vetscan HM5 hematology analyzer; Abaxis, Union City, CA, USA) for the following parameters: White blood cell (WBC) and differential leucocyte count (lymphocytes, monocytes, and neutrophils). For biochemistry, the collected blood samples were incubated at 25 °C for 30 min and centrifuged at 3000 rpm for 10 min. The sera (supernatant liquids) were stored at −20 °C prior to analysis. To confirm E2 concentration in rat sera, a competitive enzyme-linked immunosorbent assay (ELISA) (rat estrogen ELISA kit; MBS7606809; MyBioSource, San Diego, CA, USA) was performed according to manufacturer instructions. Briefly, the 96-well microplate provided in the kit had been precoated with a specific antibody. Standards and sera were then added to the appropriate wells with a biotin-labeled specific antibody. After incubation, the wells were washed and then incubated with conjugate solution attached to horseradish peroxidase. After washing, the tetramethylbenzidine substrate was added to each well, and the plate was incubated in the dark for 15 min at 37 °C. The reaction was suspended with stop solution, and the absorbance at 450 nm was measured in each well with a microplate reader (AMR-100; Allsheng, Hangzhou, China). Final concentrations were calculated using

calibration curves.

2.9. Histopathological analysis

For histopathologic analysis, skin was collected form MN insertion sites and then the skin piece was embedded in optimal cutting temperature (OCT) compound (FSC 22 Clear; Leica Biosystems, Germany). Cryosectioning of frozen tissue was performed using a cryomicrotome (Leica CM1860 cryostat; Leica Biosystems, Wetzlar, Germany) to obtain 8-μm thick slices. The skin sections were stained with hematoxylin and eosin according to standard procedures used for histologic analysis under an optical microscope (Eclipse TS100; Nikon, Japan).

2.10. In vitro placental growth factor (PlGF)- and testosterone (T)-capture tests using immuno-functionalized nMN arrays for multiplex biosensing

For PlGF-capture tests, each PAH-coated nMN patch was treated with 20 μg mL^{-1} of anti-PlGF antibody (rabbit PlGF polyclonal antibody; MBS2006779; MyBioSource) in carbonate buffer (2 μL per needle), followed by incubation for 1 h. The nMN patches were then washed six times with PBST and treated with 2 μL of BSA per needle. The nMNs were then treated with 2 μL of 0 ng mL^{-1} to 1 ng mL^{-1} PlGF (rat PlGF-1; Peprotech, Rocky Hill, NJ, USA) dissolved in PBS per needle and incubated for 1 min. The MN patch was then washed six times with PBST to remove any excess, followed by treatment of each MN with 20 μg mL^{-1} of Fluorescein isothiocyanate (FITC)-labeled secondary antibody [FITC-2^{nd} Ab; goat anti-Mouse IgG (H + L) cross-adsorbed secondary antibody, FITC; Invitrogen] in PBS (2 μL per needle) and incubated for 1 h. The MN patch was then washed six times in PBST to remove unbound antibodies. For T-capture tests, 20 μg mL^{-1} of the anti-T antibody [testosterone antibody (5E801); Santa Cruz Biotechnology] in carbonate buffer, 0 ng mL^{-1} to 25 ng mL^{-1} of T solution included in the T ELISA kit (rat testosterone ELISA kit; MBS282195; MyBioSource), and 20 μg mL^{-1} of Alexa Fluor 350 (AF350)-labeled secondary antibody [AF350-2^{nd} Ab; goat anti-mouse IgG (H + L) cross-adsorbed secondary antibody, Alexa Fluor 350; Invitrogen] in PBS were used instead of the anti-PlGF antibody, PlGF, and FITC-2^{nd} Ab, respectively.

2.11. Fluorescence analysis

Fluorescent 2^{nd} Ab (or TR-dex) bound to the nMN surface was visualized by fluorescence microscope (Eclipse TS100; Nikon), and fluorescence intensity was measured using ImageJ software (National Institutes of Health, Bethesda, MD, USA). The fluorescence intensity on the centerline across the MN was measured, and a graph of fluorescence intensity according to the position on the nMN was prepared, integrated, and averaged (Fig. S2). For fluorescence measurements using a portable fluorescence microscope, the biomarker-captured nMN array following fluorescent-2^{nd} Ab treatment was loaded onto the sample stage of the microscope, and then the top-view fluorescence image of the nMN array was taken with a smartphone camera (iPhone 6S+; Apple, Cupertino, CA, USA) after passing through a bandpass filter (500–550 nm, FF03-525/50-25; IDEX Health & Science, Henrietta, NY, USA) and an imaging lens (#49–839; Edmund Optics, Barrington, NJ, USA) (Fig. S3).

2.12. Statistical analysis

Data were analyzed using Student's *t*-test with Excel software (Microsoft Corp., Redmond, WA, USA) and expressed as the mean ± standard deviation (SD) of independent experiments. P-values < 0.05 indicate statistically significant differences.

3. Results and discussion

3.1. Fabrication of nMN arrays by electrochemical anodization

To prepare a nanoporous structure on MNs, we performed electrochemical anodization of micromachined Al MN arrays. The anodization of Al and its alloys has been intensively exploited to fabricate a self-ordered porous oxide layer in a large area (Lee and Park, 2014). The nanoporous structure of AAO, including pore diameter and oxide-layer thickness, can be precisely controlled by manipulating anodization conditions. As shown in Fig. 2a, Al MNs were electropolished to smoothen the surface, followed by anodization to form the nanoporous structure. The Al MN arrays (8 × 8 MNs cm^{-2}) were manufactured by micromachining into a bullet shape with a base diameter of 250 μm, a length of 700 μm, and tip angle of 45°. Based on MN geometry and dimension, the bullet-shaped MNs could be inserted into the skin without significant tissue damage (An et al., 2018; Seong et al., 2017), thereby offering a higher surface area as compared with typical conical MNs. Electropolishing of the micromachined MN arrays was performed for 30 s to minimize dimensional changes in the MNs (Table S1). Two-step anodization of highly pure Al (≥ 99.99%) is typically recommended to obtain uniform hexagonally ordered nanopores aligned to the Al surface; however, because two-step anodization involves selective dissolution of the porous AAO layer formed by the initial anodization step, which affects structural changes, and pure Al is too soft to manufacture into a sharp microstructure, we used one-step anodization with Al alloys containing < 5% impurities to prepare Al nMNs. A relatively regular nanoporous structure on the surface of the MN was formed in the optimized anodization condition, whereas irregular pores were observed on the AAO surface in some areas likely due to the different oxidation rates of the Al alloys during anodization (Fig. S4) (Zaraska et al., 2010). After optimized pore-widening steps (Fig. S5), we ultimately observed formation of a nanoporous AAO layer (pore diameter: ~40 nm; center-to-center distance between pores: ~85 nm; and thickness: ~15 μm) on the surface of the MNs (Fig. 2b and c). The estimated surface area of the nMNs was over 300 times greater than that of non-porous MNs (Fig. S6). To investigate the effect of morphological changes on the ability of the MN to penetrate the skin, we compared the insertion force of the MNs into porcine skin in terms of the introduction of the nanoporous structure (Fig. 2d). The nMN showed a similar insertion force to that of the non-porous MN, indicating that the nanopore-formation process by anodization did not cause a significant structural change. The nMN array was subsequently used for biomarker capture following surface functionalization with antibodies.

3.2. Immuno-functionalization of the nMN for biomarker capture

Immunoassays using antibody-antigen affinity are powerful analytical methods that exhibit high sensitivity and specificity (Kojima et al., 2003; Mak et al., 2005; Meyerhoff et al., 1995; Ronkainen-Matsuno et al., 2002). Among immunoassay methods, non-competitive sandwich immunoassays are considered a suitable format for detecting physiologically active substances with a low molecular weight, such as steroids or hormones (Gonzalez-Techera et al., 2007; Kobayashi and Goto, 2001). To capture E2 as a PE biomarker from ISFs, the surface of nMNs was immuno-functionalized (Fig. 3a). After O_2 plasma treatment of Al nMN arrays to form a negatively charged surface, the plasma-treated AAO surface was coated with a cationic polyelectrolyte (PAH) to immobilize a probe antibody (1^{st} Ab) for capturing E2 by electrostatic attraction, as the 1^{st} Ab has an isoelectric point of ~7 that exhibits a negative charge in carbonate buffer (pH 9.4). We subsequently measured the surface charge of the modified AAO layer and the 1^{st} Ab in buffers at different pH levels (Fig. 3b). The 1^{st} Ab-immobilized nMN was incubated in BSA solution to prevent nonspecific binding of target analytes on the nanoporous layer. After surface modifications, the surface morphology of the nMN was characterized by FE-SEM (Fig. 3c),

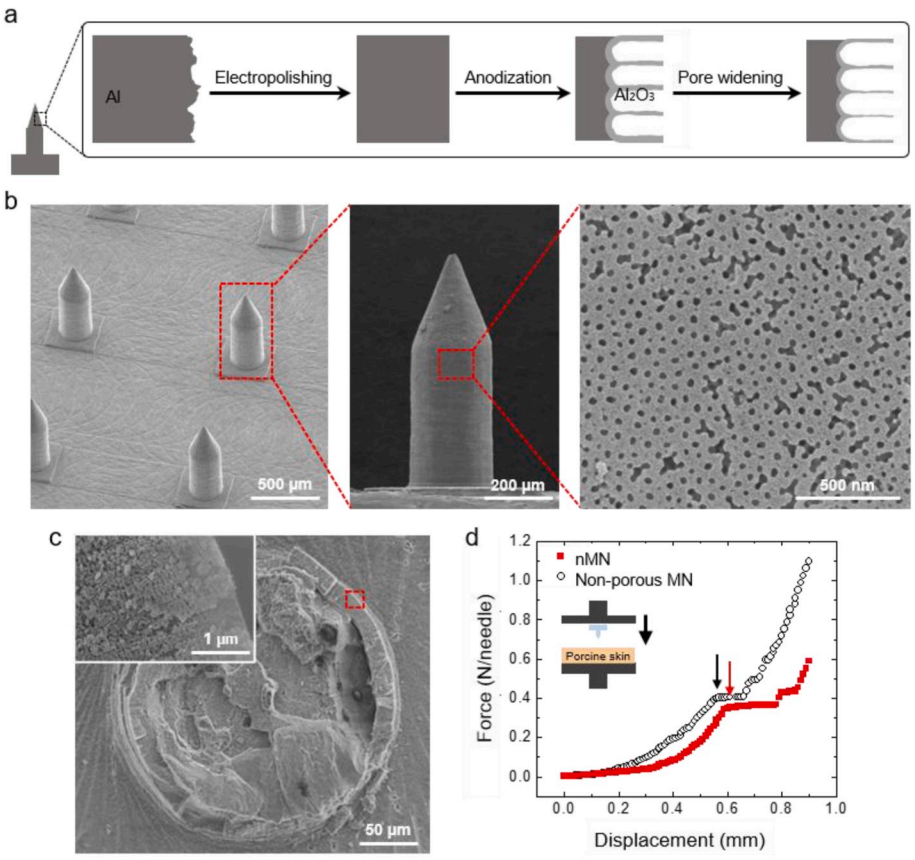

Fig. 2. Fabrication of the Al nMN for biomarker capture by anodization and pore widening. (a) Schematic illustration showing the anodization process for fabrication of the nanoporous structure on the Al MN. (b) FE-SEM images showing the array of anodized MNs (left) and the nanoporous structure formed on the MN surface (right). (c) Top-view FE-SEM images of a broken nMN showing the porous AAO layer. The average nanopore diameter and height were ~40 nm and ~15 μm, respectively. (d) Force-displacement curves obtained from insertion of the nMN and non-porous MN into porcine skin, respectively.

which revealed that as each surface modification progressed, the pore diameter of the AAO layer became smaller (down to 20 nm), whereas pore blocking was not observed. Although the immobilization of 1st probe Ab can be influenced at pH levels (5–6) of skin in women (Jacobi et al., 2005), the immobilized 1st Abs were stably retained in an acidic solution (pH 5), due to possibly increased molecular interaction and entrapment effect inside nanochannels (Fig. S7).

To develop an immunoassay platform using the nMN arrays, we investigated optimal conditions for E2 capture depending on the concentration of the immobilized 1st Ab. The nMN array (1 × 5 MNs) was incubated in 1st Ab solutions of different concentrations (10 μg mL^{-1}, 20 μg mL^{-1}, and 50 μg mL^{-1}). After washing the non-immobilized 1st Abs and BSA coating, the nMN arrays were treated with 10 ng mL^{-1} E2, which represents the normal concentration in healthy pregnant women (Shin et al., 2018). The captured E2 concentration was determined using the TR-2nd Ab. When the 1st Ab concentration was > 20 μg mL^{-1}, the fluorescence intensity of the TR-2nd Ab from the nMNs was saturated, suggesting maximal immobilization of the 1st Ab (Fig. 3d). Therefore, we used 20 μg mL^{-1} of the 1st Ab to prepare the immuno-functionalized nMN. Notably, we found that the biomolecules used for the dose-response study (i.e., 1st Ab and TR-2nd Ab) showed stable binding characteristics to the nMN surface during repeated washing steps.

Because rapid detection is desired for point-of-care testing (POCT) devices and clinical settings, we evaluated the detection capability of the nMN depending on incubation time (Fig. 3e). The 1st Ab-immobilized nMN arrays were treated with E2 solutions (1 ng mL^{-1} and 10 ng mL^{-1}) for different incubation times (1, 10, and 30 min), and their capturing ability was characterized using the TR-2nd Ab. The fluorescence intensity of the TR-2nd Ab increased along with incubation time and E2 concentration. Interestingly, even at a short incubation time of 1 min, E2 at 1 ng mL^{-1} (the lower level present in women with PE) was detected by fluorescence measurement (Fig. 3f). To determine the detection limit of the nMN for the E2 biomarker, we investigated the dose-response (E2–TR-2nd Ab) relationship using a sandwich immunoassay by characterizing the fluorescence of the nMNs (Fig. 3g and h). Infiltration of 2nd Ab into the porous structure of the MN was confirmed by the cross-sectional image of the MN after all processes (Fig. S8). We found that the nMN exhibited a linear relationship on a logarithmic scale between E2 concentration and fluorescence from the TR-2nd Ab in a range of 0.5 ng mL^{-1} to 1000 ng mL^{-1} E2. Since the uniformity of nanoporous structure on the MN surface can be improved by using two-step anodization of Al, target biomarkers can be detected more consistently and reliably using the nMN-based biosensing platform. Notably, immuno-functionalized nMN arrays demonstrated a rapid capture capability and clear difference in fluorescence at between 1 ng mL^{-1} and 10 ng mL^{-1} E2, which is the required sensitivity for PE diagnosis. By contrast, no fluorescence was detected from non-porous MN arrays, even at high E2 concentrations (1000 ng mL^{-1}), highlighting the importance of the nanoporous structure for biomarker capture (Fig. S9). In an extended incubation period (30 min), sub-nanogram-level sensitivity of up to 50 pg mL^{-1} E2 was achieved, demonstrating a possible method for increasing the detection limit (Fig. S10). Based on these experimental results, calibration curves for the E2 concentration were generated at each incubation time.

To confirm biomarker capture by nMNs through selective interaction between the E2 biomarker and the 1st Abs, we assessed two possible interaction modalities: nonspecific binding or trapping of the fluorescent TR-2nd Ab in the nanoporous AAO layer. To investigate the nonspecific binding of the TR-2nd Abs, 1st Ab-immobilized nMN arrays were treated with TR-2nd Ab solution in the absence of E2 incubation, revealing no fluorescence at the tested concentration ranges (Fig. 3i). Moreover, treatment of the nMNs with TR-dex at a similar molecular weight as the 2nd Ab also resulted in no fluorescence, highlighting the selective sensing capability of the nMNs (Fig. 3j).

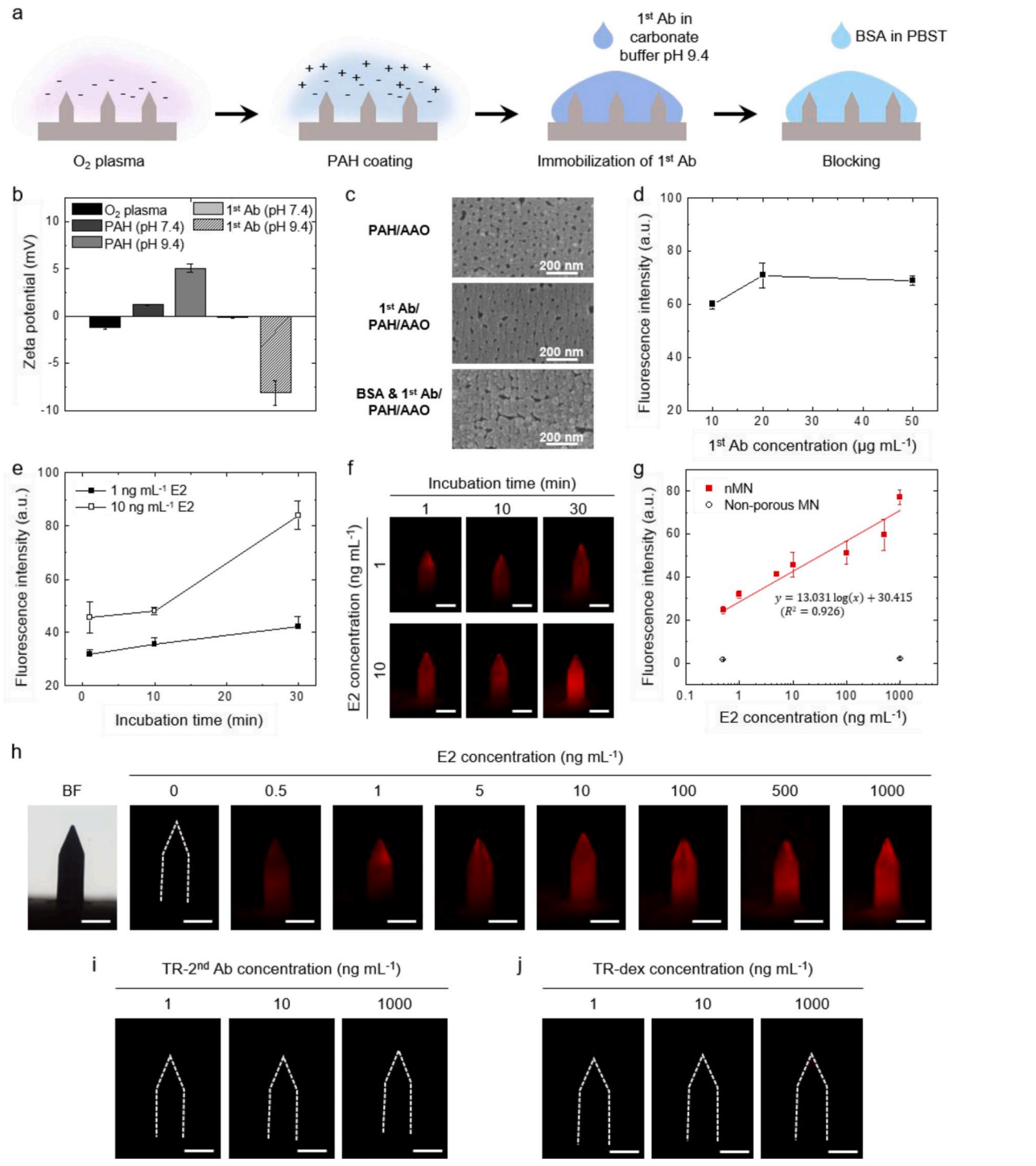

Fig. 3. (a) Schematic illustration of Al nMN surface modification for immuno-functionalization. (b) Zeta potential of anodized nanoporous Al sheets under different surface conditions. The surface charge of nanoporous Al sheets measured following sequential surface modification by O_2 plasma, PAH coating (at pH 7.4 and pH 9.4), and transfer to 1st Ab solution (at pH 7.4 and pH 9.4) under different pH conditions ($n = 3$). (c) FE-SEM images of the top surface of the nMN after sequential surface functionalization by PAH coating, 1st Ab immobilization, and BSA coating. (d) Fluorescence intensity of the TR-2nd Ab on nMNs at different immobilized concentrations of 1st Ab. The optimal concentration of 1st Ab for capturing E2 using the nMN was 20 μg mL^{-1} ($n = 5$). (e and f) Fluorescence intensity of the TR-2nd Ab on the nMN surface according to incubation time. The nMN was treated with 1 ng mL^{-1} and 10 ng mL^{-1} of E2, respectively, resulting in increases in fluorescence intensity along with incubation time ($n = 5$). (g and h) Fluorescence intensity of the TR-2nd Ab according to E2 concentration. In the case of nMN, higher E2 concentrations resulted in increased fluorescence intensity on the nMN ($n = 5$). (i) Fluorescence measurements of immuno-functionalized nMNs after incubation with TR-2nd Ab. No fluorescence was observed, highlighting the sensitivity of the nMN from selective binding of E2. (j) Fluorescence measurements of the immuno-functionalized nMN after incubation with TR-dex solution. No fluorescence was observed, indicating no absorption or trapping of fluorescent molecules. Scale bar represents 250 μm.

3.3. Biosensing efficacy of immuno-functionalized nMN patches in a pilot study

We then used experimental animals to examine the *in vivo* biosensing capability of the nMNs for E2 and its biological safety regarding an inflammatory response. To ensure reliable sensing performance of the nMN patches, the shaved dorsal area of anesthetized rats was exposed using a heating lamp for 10 min to increase blood circulation prior to nMN application. This procedure caused a temporary rise in the temperature of the skin surface (Fig. 4a). The immuno-functionalized nMN array (1 × 5 MNs) embedded in a PDMS pad was attached to a hydrocolloid adhesive (3 × 3 cm^2) for skin adherence (Fig. S1). The immuno-functionalized nMN patch was then applied to the pretreated dorsal skin of rats for 1 min (Fig. 4b, inserted), followed by its removal (Fig. 4b, removed). The puncture marks disappeared within 30 min of removing the nMN patch, with no inflammatory responses, such as redness or swelling, observed at the patch site (Fig. 4b, recovered).

The nMN patches were washed after a 1-min application onto normal and E2-injected rats, and fluorescence of the each nMN array was measured following TR-2^{nd} Ab treatment. The fluorescence intensity of the nMNs was converted to E2 concentration using the correlation equation estimated by the dose-response assays. The nMN array showed distinct differences in E2 levels between normal (0.1 ± 0.06 ng mL^{-1}) and E2-injected rats (0.6 ± 0.1 ng mL^{-1}), whereas E2 was not detected on either non-porous MNs or nMNs without a 1^{st} Ab, indicating selective binding affinity with E2 (Fig. 4c). To compare diagnostic performance, we analyzed serum samples collected from normal and E2-injected rats using commercially available ELISA kits (Fig. 4d). The E2 concentrations in serum from normal and E2-injected rats were 0.3 ± 0.02 ng mL^{-1} and 0.5 ± 0.02 ng mL^{-1}, respectively. Although intravenous injection of E2 did not make a significant difference in E2 levels in serum due to its rapid metabolism in blood (Kirdani et al., 1972), the nMN patch showed comparative sensing performance with that of ELISA kits, indicating its potential for painless diagnostic evaluation without blood collection.

To confirm the biological safety of the nMN array for live-animal skin tissue, we performed histopathologic and clinical pathologic assessments. Histopathology images collected at the nMN-insertion site revealed no remarkable changes or inflammatory cell infiltration as compared with normal rat skin (Fig. 4e and f).

To assess clinical pathology, we examined the effect of nMN application on the inflammatory response using known inflammation-specific markers. Compared with no treatment group, MN treated groups (non-porous MN and nMN) were confirmed that the WBC value was about 2 times higher (Table 1). However, there were no significant findings on the inflammatory response and all biomarker values were within the normal range (Han et al., 2010; Lee et al., 2012), suggesting that the nMN patch used for biomarker capture was biologically safe to use. Although the metal MN could induce an allergenic response, the AAO layer elicited only a minimal inflammatory response upon implantation in previous studies (Hoess et al., 2007).

As shown in Fig. 5, compared with previous MN-based diagnostic sensors having detection ranges in the microgram-level (Bollella et al., 2019; Chang et al., 2017; Ciui et al., 2018; Gholami et al., 2019; Gowers et al., 2019; Jin et al., 2019; Keum et al., 2015; Li et al., 2015b; Mohan

Table 1
Hematology values associated with inflammatory responses.

Group	WBC (10^3 μL^{-1})	LYM (10^3 μL^{-1})	MON (10^3 μL^{-1})	NEU (10^3 μL^{-1})
No treatment	4.76 ± 1.27	3.84 ± 1.40	0.07 ± 0.04	0.84 ± 0.18
Non-porous MN	8.77 ± 2.72	7.36 ± 2.37	0.12 ± 0.08	0.14 ± 0.06
nMN	8.66 ± 2.68	7.41 ± 2.40	0.14 ± 0.06	1.10 ± 0.45

LYM; lymphocyte, MON; monocyte, NEU; neutrophil.

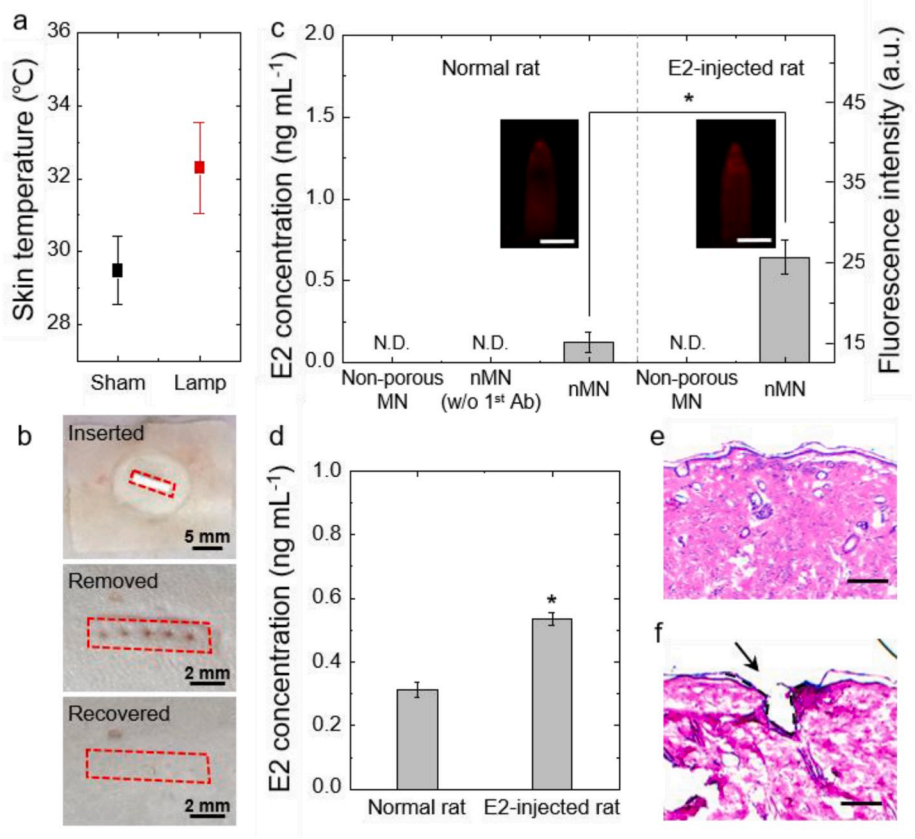

Fig. 4. *In vivo* E2 capture using MN patches. (a) The shaved dorsal skin temperature of rats under the sham condition or following heating lamp exposure. (b) Images taken following MN insertion, removal, and recovered rat skin (dotted red line). (c) E2 concentrations in normal and E2-injected rats captured by MN patches and the fluorescence intensity of the TR-2^{nd} Abs on the MN (n = 3). (d) Serum levels of E2 in both rat groups used for *in vivo* E2-capture tests, as measured by commercial ELISA kits (n = 3). Hematoxylin and eosin staining of rat skin tissue (e) before and (f) after MN insertion. The MN-insertion site is indicated by the arrow. *$p < 0.05$. Scale bar represents 250 μm. (For interpretation of the references to colour in this figure legend, the reader is referred to the Web version of this article.)

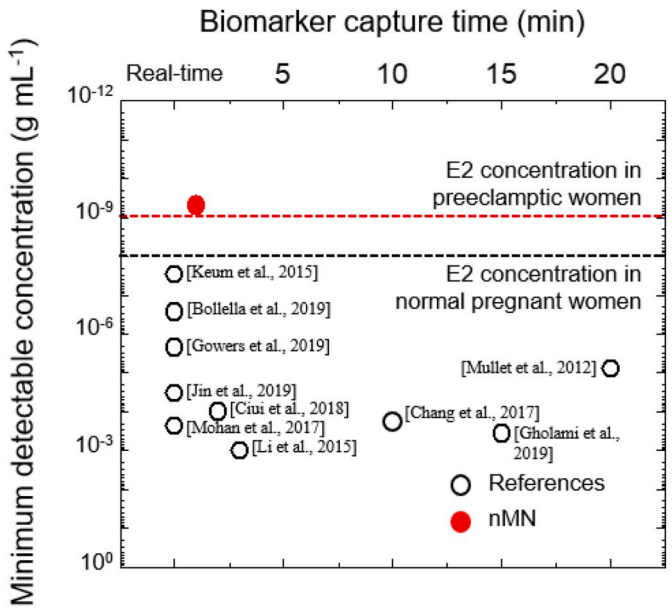

Fig. 5. Comparison of biomarker-capture time and detection limit between previous MN-based biosensors (black open circles) and the nMN-sensing platform (red closed circles) described in this study. Dashed lines indicate E2 concentrations for normal (10 ng mL^{-1}, black dotted line) and preeclamptic (1 ng mL^{-1}, red dotted line) women, respectively. (For interpretation of the references to colour in this figure legend, the reader is referred to the Web version of this article.)

et al., 2017; Muller et al., 2012), the nMN platform described in this study demonstrated superior sensitivity for diagnosis of PE according to biomarkers present in the body at nanogram or picogram levels. The rapid capture (< 1 min) of target biomarkers is advantageous for application of the nMN patches for POCT systems requiring rapid, on-site diagnosis.

To develop a multiplex biosensing platform, we integrated three different immuno-functionalized nMN arrays in a single patch to allow capture of multiple biomarkers [E2, PlGF (Krauss et al., 2004; Sunderji et al., 2010), and T (Acromite et al., 1999; Laivuori et al., 1998; Troisi et al., 2003)] associated with PE diagnosis (Fig. 6a). Each nMN array functionalized with 1st Ab for target biomarkers was used for biosensing following application of 2nd Abs with different fluorescence labels (TR-2nd Ab for E2, FITC-2nd Ab for PlGF, and AF350-2nd Ab for T). The nMN platform exhibited concentration-dependent sensing capability for detection of PlGF and T at sub-nanogram levels (Fig. 6b and c). Specifically, the limit of PlGF detection by the nMN array was 50 pg mL^{-1}, which was substantially lower than that of previous MN-based protein-sensing methods (~10 μg mL^{-1}) (Muller et al., 2012). In addition to detecting multiple biomarkers using a single patch, when the nMN array is immuno-functionalized with the same probe antibody, the nMN array could provide 2D spatial information on the concentration of the target biomarker.

To develop a nMN-based POCT platform, we measured the fluorescence of the PlGF-captured nMN array following FITC-2nd Ab treatment using a portable fluorescence microscope installed on a smartphone (Fig. 6d and e; and S3).The customized fluorescence-imaging device comprised a laser diode with a laser filter, a bandpass filter, and an imaging lens capable of detecting green fluorescence (FITC) from the immuno-functionalized nMN array treated with PlGF and FITC-2nd Ab (Fig. 6f). This smartphone-based multi-channel fluorescence-detection device can be applicable for multiplex sensing of biomarkers to

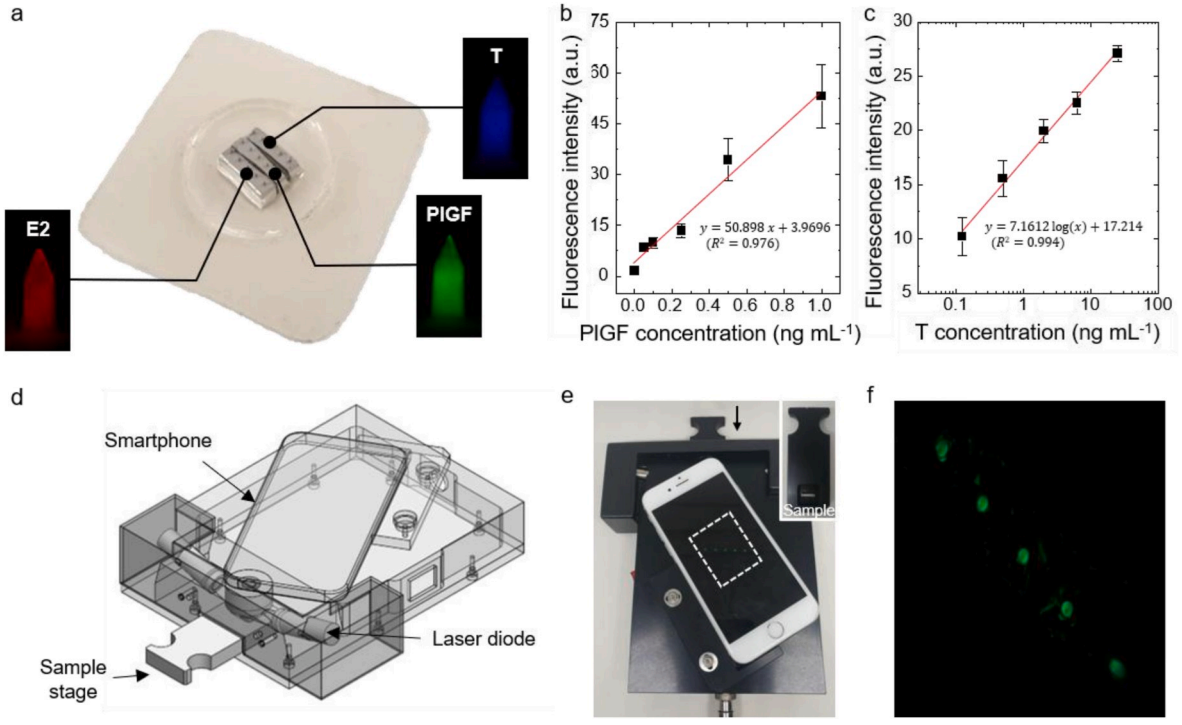

Fig. 6. (a) A multiplex biosensing patch using immuno-functionalized nMN arrays. Each nMN array was functionalized with 1st Abs for capture of target biomarkers: E2 (red), PlGF (green), and T (blue). (b and c) Concentration-dependent fluorescence intensities of (b) FITC-2nd Ab (green) and (c) AF350-2nd Ab (blue). (d) Schematic drawing and (e) photo images of portable smartphone-based fluorescence microscope for imaging of the biomarker-captured nMN arrays. A PlGF-captured nMN array following FITC-2nd Ab treatment was loaded onto the sample stage of the microscope after detachment from the backing adhesive. (f) Captured image taken from the smartphone showing the fluorescence of the PlGF-captured nMN array. (For interpretation of the references to colour in this figure legend, the reader is referred to the Web version of this article.)

increase the reliability of PE diagnosis.

4. Conclusions

We demonstrated a highly sensitive and painless POCT platform for PE diagnosis using nMN patches prepared by electrochemical anodization of Al MNs. The nanoporous structure on the MN surface enhanced biomarker capture by increasing the surface area and allowed identification of the optimal concentration for the immobilized probe antibody on the Al MN surface necessary for capturing E2 as an important PE-related biomarker. Remarkably, the immuno-functionalized nMNs were able to quickly capture biomarkers within 1 min after MN application, possibly due to fast infiltration of body fluids into nanoporous structure and increased molecular interaction between 1st probe Ab and biomarkers in the nanopores. The E2 concentrations detected by the nMN patches ranged from 0.5 ng mL^{-1} to 1000 ng mL^{-1}, similar to those reported by commercial ELISA kits. Moreover, *in vivo* experiments using normal and E2-injected rats demonstrated the ability of nMN to rapidly capture E2 in dermal ISFs, as well as its biological safety according to absence of an inflammatory response. To the best of our knowledge, this is the first report using painless MN patches to show sub-nanogram sensitivity of blood analysis levels. The immuno-functionalized nMN arrays were able to detect a variety of PE-related biomarkers, suggesting the possibility of multiple sensing platform by using a single patch with nMN arrays capable of capturing different biomarkers. These results highlighted the ability of the bio-functionalized nMN array to rapidly detect biomarkers present at sub-nanogram levels and its efficacy as a platform capable of detecting biomarkers for disease diagnosis, including PE.

Declaration of competing interest

The authors declare that they have no known competing financial interests or personal relationships that could have appeared to influence the work reported in this paper.

CRediT authorship contribution statement

Ye-Eun Kang: Conceptualization, Investigation, Writing - original draft. **Keum-Yong Seong:** Methodology, Investigation. **Sang-Gu Yim:** Methodology, Investigation. **Yechan Lee:** Methodology, Investigation. **Sung-Min An:** Methodology, Investigation. **Seung Chul Kim:** Writing - review & editing, Investigation. **Kyujung Kim:** Writing - review & editing, Investigation. **Beum-Soo An:** Writing - review & editing, Investigation. **Kyu-Sup Lee:** Writing - review & editing, Investigation. **Seung Yun Yang:** Conceptualization, Supervision, Writing - review & editing.

Acknowledgement

We thank Moon Sik Kang (NOST) for manufacturing a portable fluorescence microscope. This research was supported by the Korea Health Technology R&D Project through the Korea Health Industry Development Institute (KHIDI) funded by the Ministry of Health & Welfare of the Republic of Korea (HI16C0313) and the Basic Research Lab Program (NRF-2018R1A4A1025623) funded by the National Research Foundation (NRF) of the Republic of Korea.

Appendix A. Supplementary data

Supplementary data to this article can be found online at https://doi.org/10.1016/j.bios.2020.112281.

References

Acromite, M.T., Mantzoros, C.S., Leach, R.E., Hurwitz, J., Dorey, L.G., 1999. Am. J. Obstet. Gynecol. 180, 60–63.
An, S.-M., Seong, K.-Y., Yim, S.-G., Hwang, Y.J., Bae, S.H., Yang, S.Y., An, B.-S., 2018. Acta Biomater. 67, 238–247.
Anderson, U., Olsson, M., Kristensen, K., Åkerström, B., Hansson, S., 2012. Placenta 33, S42–S47.
Baumann, M.U., Bersinger, N.A., Mohaupt, M.G., Raio, L., Gerber, S., Surbek, D.V., 2008. Am. J. Obstet. Gynecol. 199, 266. e1–266. e6.
Bollella, P., Sharma, S., Cass, A.E.G., Antiochia, R., 2019. Electroanalysis 31, 374–382.
Bujold, E., Roberge, S., Lacasse, Y., Bureau, M., Audibert, F., Marcoux, S., Forest, J.-C., Giguere, Y., 2010. Obstet. Gynecol. 116, 402–414.
Chang, H., Zheng, M., Yu, X., Than, A., Seeni, R.Z., Kang, R., Tian, J., Khanh, D.P., Liu, L., Chen, P.A., 2017. Adv. Mater. 29, 1702243.
Chinnadayyala, S.R., Park, K.D., Cho, S., 2018. ECS J. Solid State Sci. Technol. 7, Q3159–Q3171.
Ciui, B., Martin, A., Mishra, R.K., Brunetti, B., Nakagawa, T., Dawkins, T.J., Lyu, M., Cristea, C., Sandulescu, R., Wang, J., 2018. Adv. Healthc. Mater. 7, 1701264.
Coffey, J.W., Corrie, S.R., Kendall, M.A., 2013. Biomaterials 34, 9572–9583.
Coffey, J.W., Corrie, S.R., Kendall, M.A., 2018. Biomaterials 170, 49–57.
Corrie, S.R., Fernando, G.J., Crichton, M.L., Brunck, M.E., Anderson, C.D., Kendall, M.A., 2010. Lab Chip 10, 2655–2658.
Davis, S.P., Landis, B.J., Adams, Z.H., Allen, M.G., Prausnitz, M.R., 2004. J. Biomech. 37, 1155–1163.
Gholami, S., Mohebi, M.-M., Hajizadeh-Saffar, E., Ghanian, M.-H., Zarkesh, I., Baharvand, H., 2019. Int. J. Pharm. 558, 299–310.
Gonzalez-Techera, A., Kim, H., Gee, S., Last, J., Hammock, B., González-Sapienza, G., 2007. Anal. Chem. 79, 9191–9196.
Gowers, S.A., Freeman, D.M., Rawson, T.M., Rogers, M.L., Wilson, R.C., Holmes, A.H., Cass, A.E., O'Hare, D., 2019. ACS Sens. 4, 1072–1080.
Han, Z.-Z., Xu, H.-D., Kim, K.-H., Ahn, T.-H., Bae, J.-S., Lee, J.-Y., Gil, K.-H., Lee, J.-Y., Woo, S.-J., Yoo, H.-J., 2010. Lab. Anim. Res. 26, 153–164.
Hoess, A., Teuscher, N., Thormann, A., Aurich, H., Heilmann, A., 2007. Acta Biomater. 3, 43–50.
Hwa, K.-Y., Subramani, B., Chang, P.-W., Chien, M., Huang, J.-T., 2015. Int. J. Electrochem. Sci. 10, 2455–2466.
Jacobi, U., Gautier, J., Sterry, W., Lademann, J., 2005. Dermatology 211, 312–317.
Jin, Q., Chen, H.J., Li, X., Huang, X., Wu, Q., He, G., Hang, T., Yang, C., Jiang, Z., Li, E., 2019. Small 15, 1804298.
Keum, D.H., Jung, H.S., Wang, T., Shin, M.H., Kim, Y.E., Kim, K.H., Ahn, G.O., Hahn, S. K., 2015. Adv. Healthc. Mater. 4, 1153–1158.
Kirdani, R.Y., Varkarakis, M.J., Murphy, G.P., Sandberg, A.A., 1972. Endocrinology 90, 1245–1251.
Kobayashi, N., Goto, J., 2001. Adv. Clin. Chem. 36, 139–170.
Kojima, K., Hiratsuka, A., Suzuki, H., Yano, K., Ikebukuro, K., Karube, I., 2003. Anal. Chem. 75, 1116–1122.
Krauss, T., Pauer, H.U., Augustin, H.G., 2004. Hypertens. Pregnancy 23, 101–111.
Laivuori, H., Kaaja, R., Rutanen, E.-M., Viinikka, L., Ylikorkala, O., 1998. J. Clin. Endocrinol. Metab. 83, 344–347.
Lee, J.M., Lee, M.A., Do, H.N., Song, Y.I., Bae, R.J.N., Lee, H.Y., Park, S.H., Kang, J.S., Kang, J.K., 2012. Lab. Anim. Res. 28, 115–121.
Lee, W., Park, S.-J., 2014. Chem. Rev. 114, 7487–7556.
Li, B., Wang, J., Yang, S.Y., Zhou, C., Wu, M.X., 2015a. Biomaterials 59, 30–38.
Li, C.G., Joung, H.-A., Noh, H., Song, M.-B., Kim, M.-G., Jung, H., 2015b. Lab Chip 15, 3286–3292.
Liu, F., Lin, Z., Jin, Q., Wu, Q., Yang, C., Chen, H.-J., Cao, Z., Lin, D.-a., Zhou, L., Hang, T., 2019. ACS Appl. Mater. Interfaces 11, 4809–4819.
Mak, W.C., Cheung, K.Y., Trau, D., Warsinke, A., Scheller, F., Renneberg, R., 2005. Anal. Chem. 77, 2835–2841.
Mandal, A., Boopathy, A.V., Lam, L.K.W., Moynihan, K.D., Welch, M.E., Bennett, N.R., Turvey, M.E., Thai, N., Van, J.H., Love, J.C., Hammond, P.T., Irvine, D.J., 2018. Sci. Transl. Med. 10, eaar2227.
Meyerhoff, M.E., Duan, C., Meusel, M., 1995. Clin. Chem. 41, 1378–1384.
Mohan, A.V., Windmiller, J.R., Mishra, R.K., Wang, J., 2017. Biosens. Bioelectron. 91, 574–579.
Muller, D.A., Corrie, S.R., Coffey, J., Young, P.R., Kendall, M.A., 2012. Anal. Chem. 84, 3262–3268.
O'Gorman, N., Nicolaides, K.H., Poon, L.C., 2016b. Wom. Health 12, 199–207.
O'Gorman, N., Wright, D., Syngelaki, A., Akolekar, R., Wright, A., Poon, L.C., Nicolaides, K.H., 2016. Am. J. Obstet. Gynecol. 214, 103. e1–103. e13.

Poon, L.C., Nicolaides, K.H., 2014. Prenat. Diagn. 34, 618–627.
Redman, C.W., Sargent, I.L., 2005. Science 308, 1592–1594.
Roberts, J.M., Cooper, D.W., 2001. Lancet 357, 53–56.
Roberts, J.M., Hubel, C.A., 2009. Placenta 30, 32–37.
Romanyuk, A.V., Zvezdin, V.N., Samant, P., Grenader, M.I., Zemlyanova, M., Prausnitz, M.R., 2014. Anal. Chem. 86, 10520–10523.
Ronkainen-Matsuno, N.J., Thomas, J.H., Halsall, H.B., Heineman, W.R., 2002. TrAC Trends Anal. Chem. 21, 213–225.
Seong, K.-Y., Seo, M.-S., Hwang, D.Y., O'Cearbhaill, E.D., Sreenan, S., Karp, J.M., Yang, S.Y., 2017. J. Contr. Release 265, 48–56.
Shin, Y.Y., Jeong, J.S., Park, M.N., Lee, J.E., An, S.M., Cho, W.S., Kim, S.C., An, B.S., Lee, K.S., 2018. Mol. Med. Rep. 17, 2681–2688.
Sunderji, S., Gaziano, E., Wothe, D., Rogers, L.C., Sibai, B., Karumanchi, S.A., Hodges-Savola, C., 2010. Am. J. Obstet. Gynecol. 202, 40. e41–40. e47.
Tian, M., Zhang, Y., Liu, Z., Sun, G., Mor, G., Liao, A., 2016. Sci. Rep. 6, 27683.
Troisi, R., Potischman, N., Roberts, J., Ness, R., Crombleholme, W., Lykins, D., Siiteri, P., Hoover, R.N., 2003. Int. J. Epidemiol. 32, 455–460.
Venkatesha, S., Toporsian, M., Lam, C., Hanai, J.-i., Mammoto, T., Kim, Y.M., Bdolah, Y., Lim, K.-H., Yuan, H.-T., Libermann, T.A., 2006. Nat. Med. 12, 642.
Yang, S.Y., Jeon, G., Kim, J.K., 2012. J. Mater. Chem. 22, 23017–23021.
Zaraska, L., Sulka, G.D., Szeremeta, J., Jaskuła, M., 2010. Electrochim. Acta 55, 4377–4386.